Experiments in Fluids 22 (1997) 292–299 © Springer-Verlag 1997

A combined PIV/LIF-system for the measurement of heterogeneous drag reduction effects in a pipe-flow

M. Saadeh, K. Strauss, T. Schneider

Abstract Particle Image Velocimetry (PIV) technique combined with flow visualization was applied in heterogeneous drag reduction to examine the motion of the polymer thread and the mixing process of polymer and water simultaneously at Reynolds numbers of 15000. The instantaneous velocity profiles for water/polymer motion showed in some cross-sections differences in the velocities of the two phases which indicates an interaction between the polymer thread and the water phase. The results of this interaction have not a significant effect on the drag reduction compared with the influence of the mixing process.

1 Introduction

The ability of a small amount of soluble polymer additives to reduce the friction resistance of turbulent pipe flows of Newtonian liquids is well known since the pioneering studies of Toms (1948). Many papers have indicated that a large friction modification can also be obtained by injecting a highly concentrated polymer solution into the core of the pipe flow. If the viscoelasticity of the injected polymer solution is sufficiently high, it forms a thread that preserves its density over a long distance downstream.

The first investigations of this type of drag reduction were presented by Vleggar and Tels (1973), who coined the term "heterogeneous" drag reduction. During the last years, a broad experimental and theoretical research effort has been made in order to clarify the understanding of this phenomenon and to study the possible technical application. Since the polymer thread seems to stay often in the center of the pipe, it was assumed that the drag reduction is due to an interaction between the polymer thread and the large turbulence eddies of the flow. This hypothesis has been supported by Bewersdorff and Strauss (1979), Bewersdorff (1982), Berman and Sinha (1984) and Usui (1990).

From experiments with different additives at high Reynolds numbers Hoyt and Sellin (1991) concluded that for polyacrylamide solutions, mainly the mixing process contributes to the drag reduction. They also concluded that there is a difference in the behaviour between polyacrylamide and polyethylene oxide solutions for Reynolds numbers between 10000 and 25000, where some evidence exists that under certain conditions a viscoelastic fluid thread can interact with turbulence eddies and reduce the overall friction in the pipe. Bewersdorff et al. (1993) and concluded from different experiments, that the drag reduction in a flow with an injected polymer threat of polyacrylamide is also caused by large aggregates of polymermolecules out of the threat. The influence of mixing at high Reynolds numbers was also observed for polyacrylamide by Saadeh and Strehlow (1993), who used a combination of Laser Doppler Velocimetry (LDV) and Laser Induced Fluorescence (LIF), to measure the velocity profiles for the water and the polymer phases simultaneously. Hoyer (1994) found, that the drag reduction is exclusively caused by dissolved Polymeraggregates with the threat as a source for these aggregates.

With the same technique Strehlow (1993) was able to show that the mixing process also determines the amount of drag reduction at low Reynolds numbers. Many authors e.g., Bewersdorff (1982), Usui et al. (1988), Berman (1989), showed that a Reynolds stress defect was observed in the polymer thread drag reducing system. In order to explain this effect Usui et al. (1993) investigated the motion and the deformation of the polymer thread by a flow visualization technique.

To understand the mechanism of heterogeneous drag reduction it is necessary to get more detailed information about the interaction between the polymer thread and water. Based on the disputations mentioned above, it can be concluded that it is helpful to examine the motion of the polymer thread and the mixing process of polymer and water (if it occurs) simultaneously. For this very complex kind of two-phase-flow a measurement technique is needed which allows to observe a whole flow-field at one moment. In this paper Particle Image Velocimetry (PIV) was used to study the problem mentioned above. The present technique allows to clarify the instantaneous velocity of the thread and its affecting on the velocity of surrounding water, with flow visualization. This combination has not been possible in previous technique.

Received: 31 October 1995/Accepted: 16 July 1996

M. Saadeh
Faculty of Chemical and Petroleum Engineering,
Al-Baath University, P.O. Box 77, Homs, Syria

K. Strauss, T. Schneider
Lehrstuhl für Energieprozeßtechnik und Strömungsmechanik,
Universität Dortmund, D-44221 Dortmund, Germany

Correspondence to: K. Strauss

This work was supported by AL-Baath University (Syria) and the DFG (Deutsche Forschungsgesellschaft).
Special thank is extended to Dr. A. Strehlow for the discussion and the advice given during the LIF measurements.

Particle Image Velocimetry (PIV) is described in many publications e.g., Adrian (1984), Adrian (1991), Hinsch (1993), Lourenco (1994) as an optical, non-intrusive laser technique to obtain such whole field measurements. In the recent years it became more popular in different fields of fluid mechanics because of the fast and easy evaluation of pictures due to the increased computer power as described by Willert and Gharib (1991) and Lourenco (1994). In addition to PIV in these experiments a visualization of the polymer via Laser Induced Fluorescence (LIF) is used, so it can be distinguished between the water and the polymer phase.

For the described experiments a special kind of digital PIV, which works with video-frames and cross-correlation functions for picture evaluation was employed. A short light pulse separation is necessary, otherwise the displacement of the tracer particles between two pictures caused by the fluid velocity is high compared to the observed small flow region. The normal video frequency of 25 Hz is too low for cross-correlation between two full frames. As a consequence one would use auto-correlation with double exposed video frames. This means that image shifting techniques, see Adrian (1986) and Raffel and Kompenhans (1995), like taking the pictures via a rotating mirror, are needed to determine the flow direction.

The main reason to avoid image shifting in our experiments is that the visualized polymer thread would also be shifted and could not be located unambiguously. Moreover, these techniques increase the level of complexity of the set-up, because a further spare part has to be synchronized to the capturing of the frame and they constitute an additional error source in the PIV system, as described by Raffel and Kompenhans (1995). Image Shifting causes a higher error level because of the distortion by the rotating mirror and a further step in the evaluation process by calculating of the shift velocity. Also auto-correlation brings a lower peak signal strength (Lourenco 1994) and so it is more sensitive for noise in the picture background. This caused us to design a digital PIV system, which uses the successive exposure of the two half frames of a CCD-camera working in frame-integration mode. The light pulses are triggered at the end of the first and at the beginning of the second half frame, what enables pulse separation times down to 1 ms.

2 Experimental set-up

The experimental set-up is described in Fig. 1. A Mohno pump is used to pump water from a storage tank through a surge tank (which is used to damp the pressure fluctuation of the pump) into the main pipe. This pipe was made from acrylic glass and had an inner diameter of 50 mm and a total length of 16 m. The temperature of the water was determined by a resistance thermometer mounted in the entrance section of the pipe, and the rate of flow was measured by an inductive flowmeter positioned between the pump and the surge tank. In order to measure the pressure drop, the pipe was provided with pressure taps in different positions, which could be connected in variable combinations to a differential pressure transducer. The flowmeter and the thermometer values were fed into an AT486 computer by an A/D converter. To inject the polymer solutions into the water flow with a dosing pump, a long

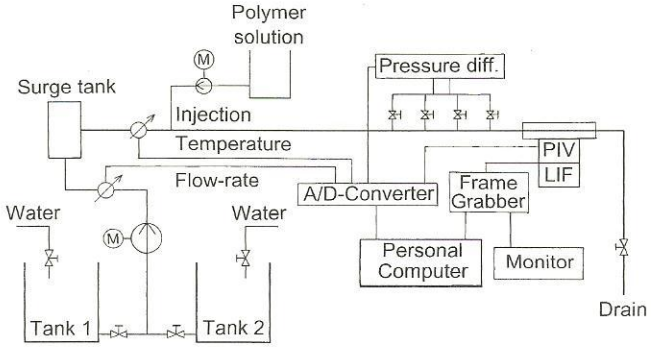

Fig. 1. Experimental setup

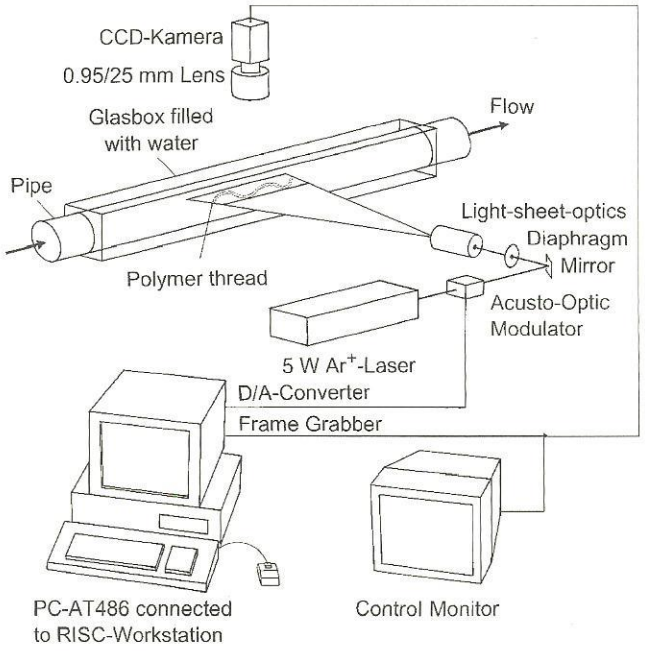

Fig. 2. Measurement section

injector was used. The optical set-up of PIV was installed at the end of the main pipe (Fig. 2).

3 Measurement technique

3.1 Principles of PIV

The principle of PIV is based on the comparing of one or two frames exposed at two different points of time t_1 and t_2. For one double-exposed picture the auto-correlation function is used to evaluate the displacement $\Delta\mathbf{x}$ in an interrogation area; for two single-exposed pictures one would use the cross-correlation function. With the magnification M of the camera, the local velocity averaged over the interrogation area is

$$\mathbf{v} = M\frac{\Delta\mathbf{x}}{t_2 - t_1} \tag{1}$$

The auto-correlation function can either be build by optical (Hinsch 1993) or digital (Willert and Gharib 1991) Fourier-transforms. The direction of the velocity vector is not unambiguous. In this case steps thus like image shifting (Lourenco 1994) must be taken, what can be avoided by using cross-correlation.

In our experiments digital cross-correlation (Chen et al. 1993) is employed. Computing the cross-correlation function needs two real-to-complex and one complex-to-complex or two complex-to-complex Fast Fourier transforms (FFT). Because of the higher calculation speed the second possibility is used. The cross-correlation function of an interrogation area of the size N times N pixels is built.

1. Calculating the Fourier transform $\hat{F}(\omega_x, \omega_y)$ of the complex N^2-array $\hat{f}(x, y)$ (x, y and ω_x, ω_y run from $-N/2$ to $N/2-1$) with the grayscale values of $g_1(x, y)$ of the first picture as the real part and the grayscale values $g_2(x, y)$ of the second picture as the imaginary part. Algorithms for the very efficient FFT can be taken from various literature, e.g. Press et al. (1992).

2. Calculating the complex power spectrum $\hat{P}(\omega_x, \omega_y)$ of the Fourier-transformed g_1 and g_2:

$$\mathrm{Re}\{\hat{P}(\omega_x, \omega_y)\} = \frac{\mathrm{Re}\{\hat{F}(\omega_x, \omega_y)\}\,\mathrm{Im}\{\hat{F}(-\omega_x, -\omega_y)\}}{2} + \frac{\mathrm{Re}\{\hat{F}(-\omega_x, -\omega_y)\}\,\mathrm{Im}\{\hat{F}(\omega_x, \omega_y)\}}{2}$$

$$\mathrm{Im}\{\hat{P}(\omega_x, \omega_y)\} = \frac{\mathrm{Re}^2\{\hat{F}(\omega_x, \omega_y)\}\,\mathrm{Re}^2\{\hat{F}(-\omega_x, -\omega_y)\}}{4} + \frac{\mathrm{Im}^2\{\hat{F}(\omega_x, \omega_y)\} - \mathrm{Im}^2\{\hat{F}(-\omega_x, -\omega_y)\}}{4}$$

$$\text{for } \omega_i \equiv -N/2 \;\Rightarrow\; -\omega_i := \omega_i \tag{2}$$

3. Re transforming the power spectrum $\hat{P}(x, y)$ via inverse Fourier-transform leads to the cross-correlation function $C(x, y)$.

The distance from the peak maximum of $C(x, y)$ to the point $(0, 0)$ gives the average displacement of the particle crowd in the interrogation spot. The position $(\Delta x, \Delta y)$ of the peak can be calculated with subpixel accuracy by fitting the peak contour around the discrete maximum (x_0, y_0) in a Gaussian error function as described by Willert (1995):

$$C(x) = C_0 \exp\left\{\frac{-(\xi - x - x_0)^2}{k}\right\} \tag{3}$$

where ξ is the subpixel distance of the real maximum from the discrete maximum and C_0 and k are curve coefficients. The fitting can be done for the y-component. To obtain the three unknowns three points (x_0-1, x_0, x_0+1) of the function are needed. This leads to

$$\xi = \frac{\ln C(x_0-1) - \ln C(x_0+1)}{2\ln C(x_0-1) - 4\ln C(x_0) + 2\ln C(x_0+1)} \tag{4}$$

Then $\Delta x = x_0 + \xi$ and $\Delta y = y_0 + \eta$, so with the known light pulse separation Δt one can calculate the velocity vector from (1).

3.2 Employed set-up

The main parts of the PIV set-up can be taken from Fig. 2. The pictures are captured with a Sony CCD-camera XC 75 CE, running in frame integration mode (see Fig. 3). In frame integration mode the frame is divided in two half frames. The first half frame is built by the odd lines (1, 3, 5, ...), the second half frame by the even lines (2, 4, 6, ...). During a capturing process of 40 ms, both half frames are successively exposed 20 ms. The camera is equipped with a Schneider Xenon 25 mm lens (#f 0.95). It is connected to a frame grabber card (Nano-Systems) in the AT486-computer, which can store four pictures of 512 · 512 8-bit pixels with a frequency of 25 Hz. The digitized pictures can be transferred to mass storage for a later evaluation. The images from the camera can simultaneously be observed on a monitor.

A 3 W Argon-ion-laser (Coherent INNOVA 70-3) is used as the light source. Because it is a cw-laser an additional device to pulse the laser light is needed. This is done by an acusto-optical modulator (A.A Opto-Electronique), which tilts the light beam in the moment, current is put on it. The tilted light beam can easily be blocked by a diaphragm. The advantage of this kind of pulse generator in comparison to a mechanical chopper, e.g. a rotating plate with two slits, is that it can be triggered by the reset signal of the CCD-camera, so there is no need to control the camera by an asynchronous reset. The reset signal at the beginning of a exposure sets a digitization action flag on the frame grabber with a delay of 20 ms (Fig. 3), which is used as the digitizing command. The modulator can be controlled by the computer via a D/A converter, so it is possible to trigger the light pulses exactly to the capturing of the picture. To produce the light sheet a special grid lens optic (Schäfter & Kirchhoff) is used. The advantage of this kind of lens compared with

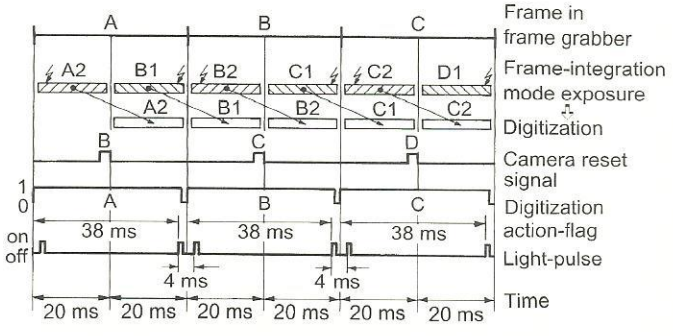

Fig. 3. Video timing diagram of the CCD-camera

a conventional cylindrical lens is, that the light sheet has a homogeneous and not a Gaussian intensity distribution over the full length.

To avoid distortions from the cylindrical surface of the pipe, a box with a square cross-section, filled with water, encloses the pipe. The camera and the light sheet are arranged perpendicular to the box. In pre-experiments it was found, that the position error as a result of the refraction can be decreased to 0.1 mm (image width 50 mm) by using the box. The light sheet is adjusted to the pipe axis and the image is filled exactly by the tube diameter.

3.3
Special exposure technique

The evaluation of double-exposed pictures via auto-correlation means the use of image shifting techniques (Adrian 1986) to avoid the ambiguity, so the advantage of cross-correlation is obviously. With expected flow velocities about $v_{max} = 0.4$ m/s and an interrogation area of $N^2 = 64 \cdot 64$ pixel^2 in a $L^2 = 512 \cdot 512$ pixel^2 image ($l^2 = 50 \cdot 50$ mm^2) captured with video frequency of 25 Hz it is not possible to use cross-correlation technique for the PIV-evaluation. So we designed a special frame capturing technique for cross-correlation evaluation which allows shorter light pulse separations. The maximum time between two images for using cross-correlation is in this case:

$$\frac{N}{2}\frac{l}{L}\frac{1}{v_{max}} \approx 8 \text{ ms} \tag{5}$$

In general it can be said, that the maximum displacement should be 1/4 of the interrogation window length, so in this case a pulse separation time of 4 ms is desirable. The pulse length should be no longer than 1 ms because stretched particle images produce a lower correlation peak signal (Willert and Gharib 1991). As previously mentioned, this is not possible by using the normal video frequency. But when a camera with successive half-frame exposure (see Fig. 3) is used the first light pulse can be given to the first and the second light pulse to the second half picture.

The synchronization of light pulsing and frame capturing is controlled by the computer, which uses the digitization signal of the frame grabber to detect the current camera status. The procedure is shown in Fig. 3. 20 ms after the first frame (A) is triggered the digitization of (A) starts which takes 40 ms. During this time the action-flag of the frame grabber is set. After 20 ms of digitization the capturing of the next frame (B) begins. So the first light pulse on half frame B1 is initialized 38 ms after the digitization started, the second light pulse on B2 4 ms later. The delay times are controlled by clock ticks of the computer. The digitized pictures are stored in the build-in memory of the frame grabber. When the capturing process is finished, the pictures are going to be transferred to harddisk drive.

For evaluation the grayscale values of the first half frame are written in $g_1(x, y)$ and those of the second half frame in $g_2(x, y)$. Because of the division in two half frames an interrogation area of $64 \cdot 64$ pixel^2 leads to data arrays of $32 \cdot 64$ values for g_1 and g_2. So the cross-correlation function has to be build in an array of $32 \cdot 64$ points also. The velocity vector can be calculated from the resulting displacement vector of the half frames $\Delta \mathbf{x}_h$:

$$\mathbf{v} = \frac{M}{t_2 - t_1}\begin{pmatrix} 2\Delta x_h + 1 \\ \Delta y_h \end{pmatrix} \tag{6}$$

The array g_2 is shifted in vertical direction by on pixel, but when the correlation function is built both arrays have the same position, so an offset of one has to be added to the doubled vertical component. The vector represents the average displacement of all the particle images in this area. The complete measuring area is $50 \cdot 50$ mm^2 and the thickness of the light sheet is about 5 mm. The distance between the vectors in x- and y-direction is 32 pixels, so the interrogation areas are overlapping 50% in each direction. Obviously wrong vectors are eliminated.

4
Measurement conditions

All measurements in this study were made at Reynolds numbers of nearly 15000. The polymer used was polyacrylamide Separan AP45 (manufactured by DOW Chemicals Inc.). The concentrated polymer solutions which had concentrations of $C_p = 3000$, 4000 and 6000 ppm, were prepared by suspending the polymer together with some aluminium tracer particles necessary for PIV and a small amount of fluorescein in isopropanol. This mixture then was added to the desired amount of deionized water and stirred gently for about 48 h. The employed injector was made from a pipe of 1 m length and 12 mm outer diameter with the possibility to adjust nozzles of different diameters at its outlet. This considerable length was chosen to avoid influences on the injection from the wake of that part of the injector which is not positioned in line with the flow direction. The inner diameters of the used nozzles were varied from 1 to 5 mm, in order to keep the injection velocity of the polymer thread nearly equal to the mean velocity of water. The measurement section was positioned at 8.5 m downstream from the injector. The drag reduction DR is calculated by comparing the friction factor of the drag reduced flow F_p with that of pure solvent F_s:

$$DR = 1 - \frac{F_p}{F_s} \tag{7}$$

5
Results

First PIV measurements were made for turbulent water flow to check the performance of the system. Therefore, aluminium particles were added to the water in tank 1. Four instantaneous velocity profiles calculated from different cross-sections of the vectorfield of a waterflow at Reynolds 15000, for axial and radial directions are shown in Fig. 4. As it can be seen, there are no significant differences between the profiles. The fluctuations in axial direction are less than 10%. It is important here to note that each vector describes the instantaneous average velocity of an area of $6.25 \cdot 6.25$ mm^2. For comparison purpose, the mean velocity profile was calculated for the measured instantaneous velocities to compare it with the velocities which were calculated from the well known formula according to

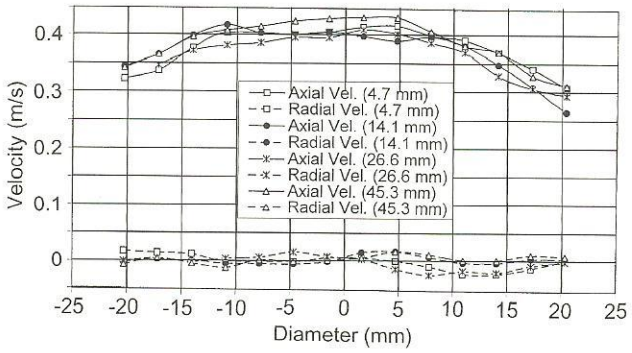

Fig. 4. Instantaneous velocity profiles for water

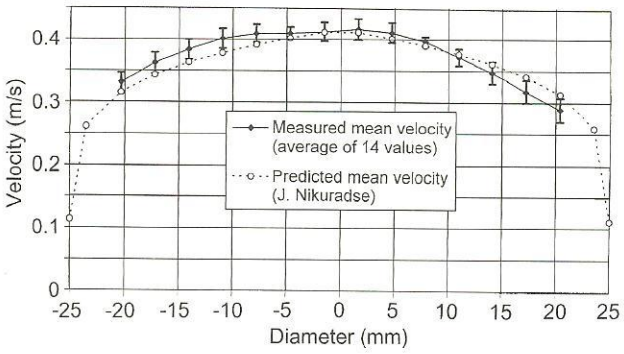

Fig. 5. Measured and predicted mean velocity profiles

Nikuradse (Schlichting 1982):

$$u(r) = U\left(1 - \frac{r}{R}\right)^{1/n} \tag{8}$$

$$U = \bar{u}\frac{(n+1)(2n+1)}{2n^2} \tag{9}$$

with

$\bar{u}$ – the measured mean velocity; $\bar{u} = 0.33$ m/s

U – the maximum velocity

R – the radius of the pipe; $R = 25$ mm

r – the distance from the axis of the pipe; $r = 0$–25 mm

$n = 6$ for $Re = 4000$

$n = 7$ for $Re = 110000$

Figure 5 shows the measured and calculated ($n = 6$) mean velocity profiles for water at a Reynolds number of 15000. Despite of the reduced data-quality due to the distortion caused by the geometry of the pipe, the measured profile looks rather smooth and shows a good agreement with the predicted profile. The error bars show the statistical error of the mean velocities. The maximum error is about 6%. The theoretical values are not more than 1% out of the confidence intervals of the measured values, so one can assume, that the complete error for the measuring of the velocity is about 10% or even less.

To proof that the injection process itself does not affect the measurements, first PIV measurements, were made for pure water flow. Then a dilute polymer solution with a polymer concentration C_p of 100 ppm, was injected into a water flow to

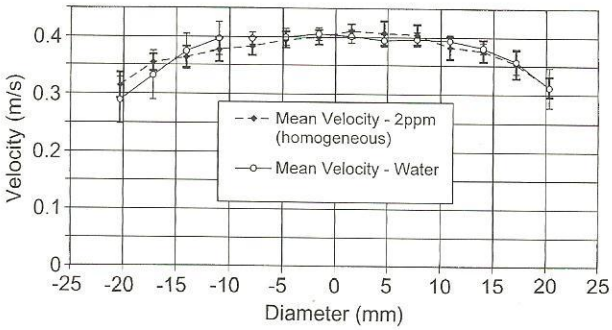

Fig. 6. Mean velocity profiles for water and homogeneous solution

reach an average polymer concentration C_{av} of 2 ppm. Due to the low concentration the polymer solution was mixed completely with mean flow when it reached the measurement section. Figure 6 shows the mean velocity profiles for pure water and homogeneous solution, calculated from 14 measured values. The confidence intervals of the two curves overlap for every measuring point, so the comparison shows that there is no significant difference between the profiles.

Since the main purpose was to detect simultaneously the motion of the injected polymer thread and the polymer distribution process, it was necessary to make sure that all the aluminium particles originate from the injection solution. Therefore, the experimental system was cleaned before each measurement using pure water (tank 2, Fig. 1), until a controlling measurement showed that nearly no particles were in the flow. Then concentrated polymer solutions containing aluminium particles and a small amount of fluorescein with various polymer concentrations C_p were injected into a pure water flow at Reynolds number of 15000 with an average polymer concentration C_{av} varying from 6.1 to 15 ppm. At a concentration C_p of 3000 ppm, the thread was disrupted by the turbulent mean flow, but its fragments kept their identity up to the end of the pipe. Figure 7 shows the instantaneous velocity vectors with flow visualization for 3000 ppm polymer solution injected with an average concentration of 10 ppm. Since the aluminium particles were added only to the polymer solution, it was clear that all the vectors originated from the polymer phase due to a mixing process. This proves, that the velocity of the polymer phase can be measured independent of the water flow. The single tracer particles in the polymer can be resolved by the evaluation algorithm, though the flourescein decreases the contrast.

To limit the influence of polymer fragments disrupted from the polymer thread, PIV measurements were made for injected concentrated polymer solutions of $C_p = 4000$ and 6000 ppm. In this case, due to the viscoelastic properties of the solutions, the polymer formed a stable thread and kept its density downstream. The results of the PIV measurements with flow visualization for injected polymer concentration of 4000 ppm, $C_{av} = 10$ ppm are shown in Fig. 8. The drag reduction DR was calculated from the pressure drop for the various amounts of injected polymer solutions. It was found that with increasing injected polymer concentration C_p or the average concentration C_{av}, the area around the polymer thread where velocities were measured decreased. In same time the drag reduction

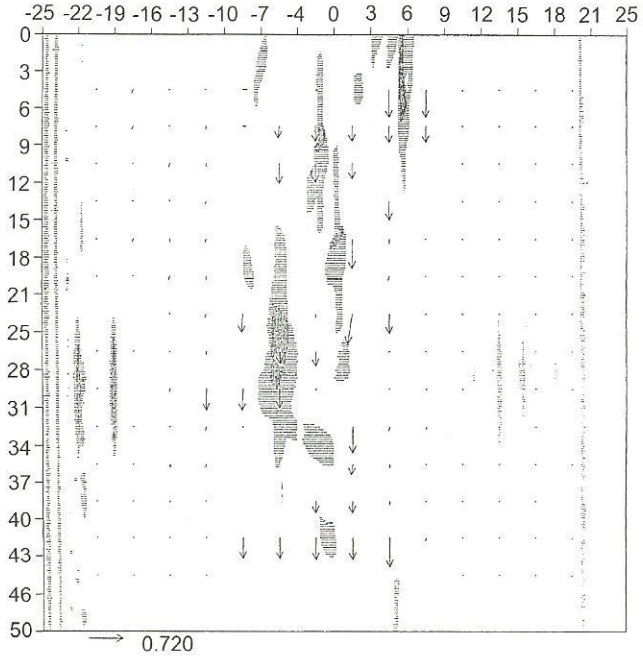

Fig. 7. Motion of visualization of the polymer phase ($C_p = 3000$ ppm)

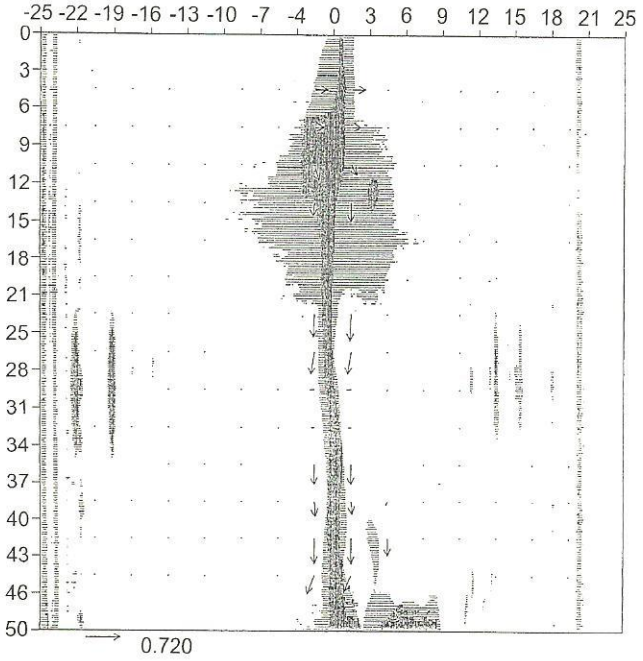

Fig. 8. Motion of visualization of the polymer phase ($C_p = 4000$ ppm)

achieved with injection of polymer solutions decreased as shown in Fig. 9.

At high average polymer concentration $C_{av} \geqslant 10$ ppm, where the rate of polymer fragments distributed in the flow is very small, it may be assumed that the vectors around the thread describe the motion of the thread itself (see Fig. 8). It can be assumed, that the error of the measured threat velocity is in the same range as the error for the water phase, because it is the

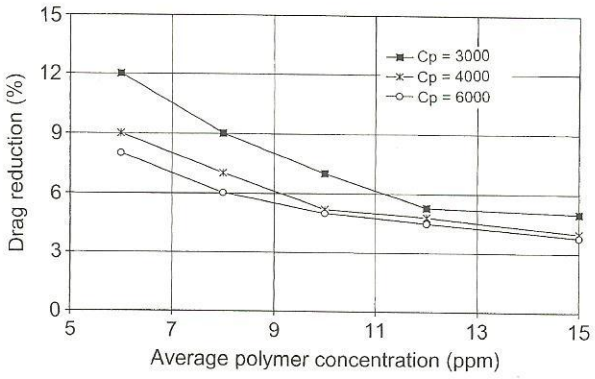

Fig. 9. Influence of the concentration of the injected polymer on the drag reduction

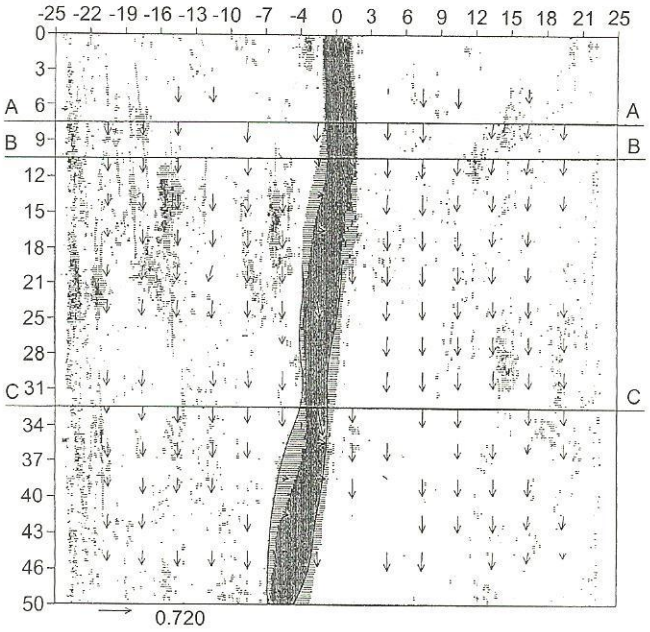

Fig. 10. Motion of water and polymer thread ($C_p = 4000$ ppm)

same measuring set-up. In the next series of experiments the particles were dispersed in the water (tank 1), as well as in the polymer solution. By adjustment of suitable conditions for PIV measurements, it was possible to measure velocities for both phases simultaneously. To identify the polymer thread in the resulting vector fields, the polymer solution was marked with a small amount of fluorescein.

The measurements for injected polymer concentration of 4000–6000 ppm show that in some positions of the thread there is a significant difference between the velocities of the two phases. Figure 10 shows the velocity vectors when a polymer solution with a concentration $C_p = 4000$ ppm was injected which corresponds to an average polymer concentration in the flow of $C_{av} = 15$ ppm. Obviously, the velocities in the vicinity of the polymer thread are very different from those in the main flow further away from the thread (see A, B, C positions in Fig. 10). In different parts of the thread radial components towards the center of the pipe can be seen. The contour of the polymer

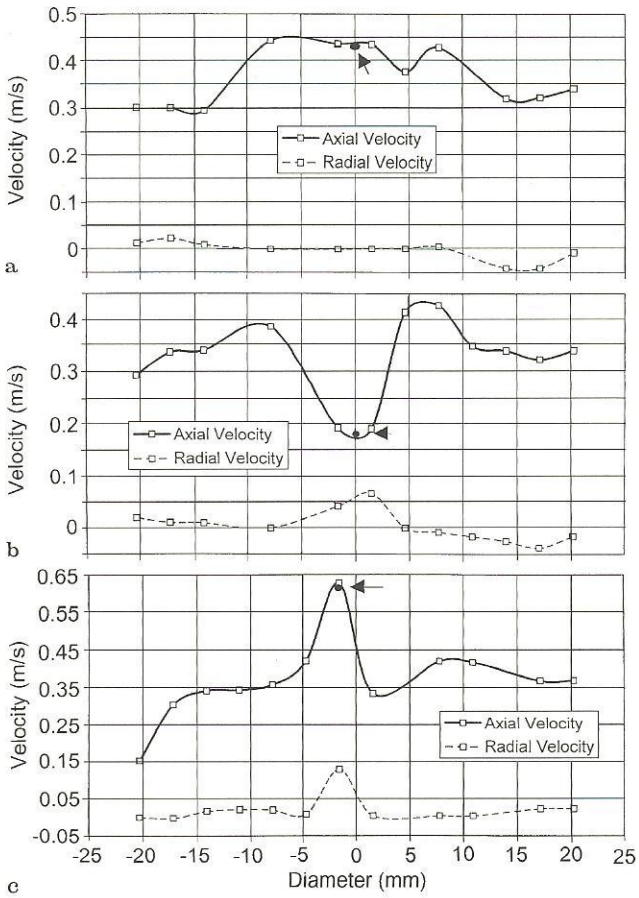

Fig. 11a–c. Instantaneous velocity profiles for water and polymer in A, B, C

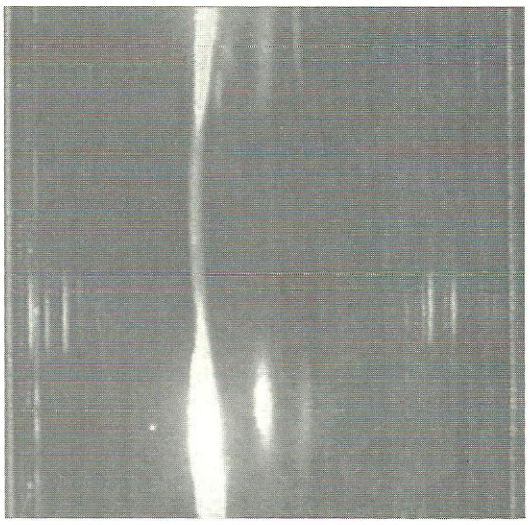

Fig. 12. Videoprint of visualization showing the elongation effect ($C_p = 4000$ ppm)

thread (Fig. 10) is signed for the first exposed half picture. In section C the diameter of the polymer thread is significantly smaller than in the other parts of the thread, and its velocity is higher than the velocity in the surrounding water. Section B shows a part, where the velocity of the thread is lower than for water. In the other positions the thread moves with a good correspondence with water (section A). The higher velocity of the thread is caused by contraction of its stretched parts further downstream. On the other hand there is a decreased velocity in the compressed thread parts. In Fig. 10 can be seen that the accelerated regions of the thread are elongated and thinned, while the regions of contraction are thicker. The fact that the different geometries of the thread correspond with the viscoelastic material behavior of the polymer solution is an indication that the thread has not moved out of the light sheet during the take. Figure 11 shows the axial and radial velocities for both phases at sections A, B and C. A further example for the elongation effects is given by Fig. 12. In this video print ($C_p = 4000$ ppm) the extreme variation of thread diameter in axial direction is obvious. The diameter in this picture varies between 2 and 4 mm, so it is smaller than the thickness of the light sheet. If this variation was caused by a displacement of the thread in the direction normal to the light plane, it would be out of the plane for more than 50%. In this case the fluorescence intensity would be much lower in the smaller parts.

6 Discussion

In spite of the fact that the time smoothed velocity for water (Fig. 5) was calculated by using only 14 measured values, the profile shows a good agreement with the well known experimental results. It was found that the average error between the profiles was 3.1%. All the experiments described above clearly indicate that a mixing process of polymer fragments substantially influences the amount of drag reduction. This results agree well with the finding of Hoyt and Sellin (1991), Strehlow (1993) and Hoyer (1994). The intensity of mixing and thus drag reduction was decreased by increasing the concentration of the polymer solution (Fig. 9). Due to this relationship between the drag reduction and the polymer concentration it can be understood that at higher Reynolds numbers homogeneous solutions are more effective than heterogeneous solutions. At high polymer concentration of the injected solutions ($C_{av} > 10$ ppm), it was found that the thread moves in the main flow nearly without mixing. In these cases only a small drag reduction was measured, and it seems to be independent from increasing the concentration of the injected polymer solutions. The observation of the deformation of the polymer thread and the simultaneous measurement of the velocities allow the conclusion that the deformation of the thread is closely related to its higher velocity. In Figs. 10 and 11 section C it is shown that close to an elongated section of the thread, its velocity is higher than in the surrounding water, which indicates an interaction between the two phases. The results of this interaction have not a significant effect on the drag reduction compared with the influence of the mixing process. Due to the elastic behaviour of the polymer there occur local differences between the velocities of the threat and the surrounding water flow.

References

Adrian RJ (1984) Scattering particle characteristics and their effect on pulsed laser measurements of fluid flow: speckle velocimetry vs. particle image velocimetry. Appl Opt 23: 1690–1691

Adrian RJ (1986) Image shifting technique to resolve directional ambiguity in double-pulsed velocimetry. Appl Opt 25: 3855–3858

Adrian RJ (1991) Particle-imaging techniques for experimental fluid mechanics. Ann Rev Fluid Mech 23: 261–304

Berman NS (1989) polymer contribution to transport equation. In: Drag reduction in fluid flows, ed. R.H.J. Sellin, R.T. Moses, pp. 21–26 Chichester: Ellis Horwood

Berman NS; Sinha PK (1984) Drag reduction in pipe flow for non-homogeneous injection of polymer additives. In: Drag reduction, Ed. R.H.J. Sellin, R.T. Moses. Univ. of Bristol, B. 3-1

Bewersdorff HW; Gyr A; Hoyer K; Tsinober A (1993) An investigation of possible mechanisms of heterogeneous drag reduction in pipe and channel flows. Rheol Acta 32: 140–149

Bewersdorff HW (1982) Effect on a centrally injected polymer thread on drag in pipe flow. Rheol Acta 21: 587–589

Bewersdorff HW; Strauss K (1979) Tyrbulente diffusion und widerstandsverminderung in rohrsrömungen. Rheol Acta 18: 104–107

Chen DJ; Chiang FP; Tan YS; Don HS (1993) Digital speckle-displacement measurement using a complex spectrum method. Appl Opt 32: 1839–1849

Hinsch K (1993) Particle image velocimetry. In: Speckle metrology, ed. R.S. Sirohi, pp. 235–324. New York: Marcel Dekker

Hoyer K (1994) Heterogene Widerstandsverminderung in turbulenten Rohrströmungen. Ph.D. Thesis 10525, Eidgenössische Technische Hochschule Zürich

Hoyt JW; Sellin RHJ (1991) Polymer threads and drag reduction. Rheol. Acta 30: 307–315

Lourenco LM (1994) Particle image velocimetry. In: Non-intrusive measurement techniques. Brussels: von Karman Institute for Fluid Dynamics lecture series 1993-09

Press WH; Flannery BP; Teukolsky SA; Vetterling WT (1992) FFT in two or more dimensions. In: Numerical recipies in C, 2nd Ed., pp. 467–470. Cambridge: Cambridge Univerisity Press

Raffel M; Kompenhans J (1995) Theoretical and experimental aspects of image shifting by means of a rotating mirror system for particle image velocimetry. Meas Sci. Technol 6: 1–14

Saadeh M; Strehlow A (1993) The influence of injection system on drag reduction. Rheol Acta 32: 398–404

Schlichting H (1982) Turbulente Rohrströmung. In: Grenzschicht-Theorie, pp. 609–648. Karlsruhe: Braun-Verlag

Strehlow A (1993) The influence of injection system on drag reduction. Ninth Symp. on Turbulent Shear Flows, Kyoto, Japan 3, P308

Toms BA (1948) Some observation on the flow of linear polymer solutions through straight tubes at large Reynolds numbers. In: Proc. 1st Int Congr. Rheol. pp. 135–141. Amsterdam: North-Holland

Usui H (1990) Structure of turbulence and drag reduction, ed. A Gyr, pp. 257–274. Berlin: Springer

Usui H; Maeguchi K; Sano Y (1988) Drag reduction caused by the injection of polymer thread into a turbulent pipe flow. Phys Fluids 31: 2518–2523

Usui H; Sakuma Y; Saeki T (1993) Reynolds stress defect in polymer drag reducing flow. Ninth Symp. on Turbulent Shear Flows, Kyoto, Japan 2 20–3

Vleggar J; Tels M (1973) Drag reduction by polymer threads. Chem Eng Sci 28: 695–968

Willert CE; Gharib M (1991) Digital particle image velocimetry. Exp Fluids 10: 181–193

Willert CE (1995) Evaluation of digital PIV recordings. In: Application of particle image velocimetry. Göttingen: Lecture series of DLR and University of Oldenburg